OPEN

Quantum confinement-induced tunable exciton states in graphene oxide

Dongwook Lee[1], Jiwon Seo[1,2], Xi Zhu[3], Jiyoul Lee[4], Hyeon-Jin Shin[4], Jacqueline M. Cole[1,5,6], Taeho Shin[4], Jaichan Lee[2], Hangil Lee[7] & Haibin Su[3,8]

[1]Cavendish Laboratory, University of Cambridge, J. J. Thomson Avenue, Cambridge CB3 0HE, United Kingdom, [2]School of Advanced Materials Science and Engineering, Sungkyunkwan University, Suwon 440-746, Republic of Korea, [3]Division of Materials Science, School of Material Sciences and Engineering, Nanyang Technological University, 639798 Singapore, [4]Samsung Advanced Institute of Technology Giheung-gu Yongin 446-712, South Korea, [5]Department of Chemistry, University of New Brunswick, P. O. Box 4400, Fredericton, NB, E3B 5A3, Canada, [6]Department of Physics, University of New Brunswick, P. O. Box 4400, Fredericton, NB, E3B 5A3, Canada, [7]Department of Chemistry, Sookmyung Women's University, Seoul 140-742, South Korea, [8]CINTRA CNRS/ NTU/THALES, UMI 3288, Research Techno Plaza, 50 Nanyang Drive, Border X Block, Level 6, Singapore 637553.

Graphene oxide has recently been considered to be a potential replacement for cadmium-based quantum dots due to its expected high fluorescence. Although previously reported, the origin of the luminescence in graphene oxide is still controversial. Here, we report the presence of core/valence excitons in graphene-based materials, a basic ingredient for optical devices, induced by quantum confinement. Electron confinement in the unreacted graphitic regions of graphene oxide was probed by high resolution X-ray absorption near edge structure spectroscopy and first-principles calculations. Using experiments and simulations, we were able to tune the core/valence exciton energy by manipulating the size of graphitic regions through the degree of oxidation. The binding energy of an exciton in highly oxidized graphene oxide is similar to that in organic electroluminescent materials. These results open the possibility of graphene oxide-based optoelectronic device technology.

The discovery of graphene in 2004 ignited prolific research owing to its potential for diverse applications, such as high speed semiconductor chips, flexible devices, optoelectronics applications, and energy storage[1–3]. Unlike graphene, which is a zero band-gap semiconductor, nano-graphene materials have a band gap. Accordingly, some of these materials exhibit optical emission due to quantum confinement effects[4]. In this way, nano-sized graphene and related materials have attracted much attention since they are expected to replace conventional cadmium-based quantum dots.

Among graphene-based materials, graphene oxide (GO) has stimulated a large body of research due to its luminescent properties. However, the origin of these properties is still controversial due to the complex structure of GO[5–8]. Here, we report for the first time that core/valence excitonic states are induced by quantum confinement in the graphitic regions of GO. Furthermore, the exciton binding energies are tuned by the degree of oxidation, i.e. the size of sp² domains.

Results

Figure 1 shows transmission electron microscope (TEM) images of two GO samples (GO1 and GO2) with different degrees of oxidation. The O:C ratios of GO samples obtained by energy dispersive X-ray (EDX) analysis are 0.35 and 0.38 for GO1 and GO2, respectively. The GO images appear as dim fringes, which are nearly straight lines, owing to the presence of overlapping GO sheets. These fringes are readily observed in sample GO1 (Figure 1a). The stripes appearing in GO2 (Figure 1b) alternate black and white, similar to that found for graphene ripples whose edges are functionalized with chemical groups[9,10]. The stripes represent flat regions that are wrinkled at their boundaries. The average stripe width in the image is 20 nm (5 stripes per 100 nm). The insets of Figure 1a and Figure 1b are the corresponding electron diffraction patterns of GO1 and GO2, respectively. These diffraction patterns can clearly be distinguished, implying that the crystalline phase is dominant. A small circular diffuse feature is also visible at the center of these diffraction patterns, revealing that GO also harbors amorphous regions. These TEM images therefore demonstrate that two spatially separated phases coexist in GO: a reacted amorphous region and an unreacted crystalline region. Figure 1c illustrates the schematic structure of GO based on these TEM images.
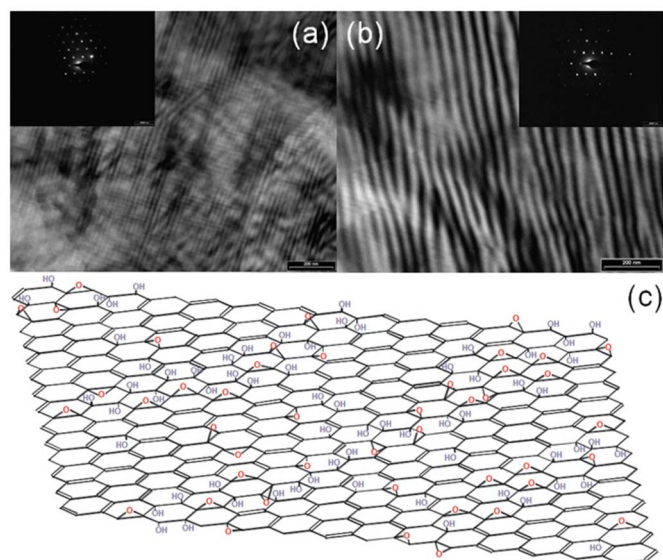
Figure 1 | TEM images of GO samples. (a) GO1 and (b) GO2. The scale bars of (a) and (b) are 200 nm. (c) Schematic structure of GO based on the TEM.

The unreacted regions are not perfectly flat, i.e. there are some functionalized chemical groups within such regions. The reacted regions act as electronic potential energy barriers between unreacted regions. Owing to the structural distinction of GO, as determined by its specific domain and oxidation characteristics, we surmise that each unreacted region acts like an individual graphene nanoribbon (GNR) or graphene nano-diamond separated by these boundary walls. If unreacted regions are properly separated by reacted regions that function as potential energy barriers, electrons in graphitic (unreacted) regions can be confined to generate electron-hole coupling, while new electronic structures can be induced by controlling the degree of oxidation in GO.

In order to confirm the presence of core excitons in GO, we performed C K-edge X-ray absorption near edge structure (XANES) measurements. Given the dielectric characteristics of GO, there was a need to circumvent potential charging problems in this XANES experiment. In order to avoid charging, the entrance to the electron detector was biased to a positive potential, effectively raising the potential of the sample surface above the ground potential. In this way, charge-compensating electrons could fill the vacant

states in GO more efficiently. The total electron yield (TEY) signal was collected as the bias voltage increased from 0 to +500 V. At 0 V bias, the peaks at 285 eV, 287 eV, and 291 eV were unclear due to charging effects. At +250 V, GO1 in Figure 2a shows four clear peaks at 285 eV, 287 eV, 288 eV, and 291 eV. The peak at 285 eV corresponds to the π* antibonding state of C=C[11]. The peak at 287 eV was assigned to the π* antibonding of C-OH[12]. The third peak at 288 eV may originate from the π* antibonding of the epoxy group (C-O-C). The fourth peak at 291 eV denotes the σ* state of C=C[11,13]. At +500 V, the peak at 287 eV (π*) becomes much sharper and increases in intensity. The shape and sharpness of this peak is typical of a core exciton, and is assigned as E_{ex}. The binding energy of the core exciton (E_B) was estimated by evaluating E_{CB}, the conduction band edge of GO1. E_{CB} was extracted by fitting the XANES spectrum with Lorentzian and arctangent functions, which describe the exciton state and the continuous step[14], respectively (Figure 2b) such that $E_B = E_{CB} - E_{ex}$. This yielded an E_B of 500 meV for GO1. Generally, the binding energy of the core exciton is larger than that of the valence exciton. The binding energy found here is much larger than that found for excitons in Si and GaAs, corresponding to 14.7 meV and 4.2 meV, respectively. However, the binding energy is similar to that found in organic electroluminescent (EL) materials (e.g. polydiacetylene (PDA) 500 meV, polythiophene (PT) 500 meV, and Tris(8-hydroxyquinolato) aluminum (Alq3) 1400 meV)[15].

The effective mass (μ) of the core exciton in GO1 with a binding energy was obtained by,

$$\mu = \frac{E_B}{R_H} * \varepsilon_r^2 * m_0, \qquad (1)$$

where R_H is the Rydberg energy (13.6 eV), ε_r is the dielectric constant of GO (ca. 2.31 at room temperature[16]), and m_0 is the electron rest mass. Thus, the effective mass of a core exciton in GO1 is μ = 0.196 m_0. The Bohr radius of this core exciton (a_x) can also be calculated with the following equation,

$$a_x = \frac{\varepsilon_r}{\mu} * a_H * m_0, \qquad (2)$$

where a_H is the Bohr radius (0.529 Å). Equation (2) leads to an exciton Bohr radius (a_x) in GO1 of about 6.23 Å, implying that core excitons are localized in GO1.

In the same way as for GO1, the Bohr radius of the core exciton in GO2 was obtained. The Bohr radius, the effective mass, and the binding energy of these core excitons are presented in Table 1, together with the O:C ratios of GO samples. As the O:C ratio increases, the binding energy of the exciton increases, while the Bohr radius decreases. An increasing O:C ratio produces more chemical groups
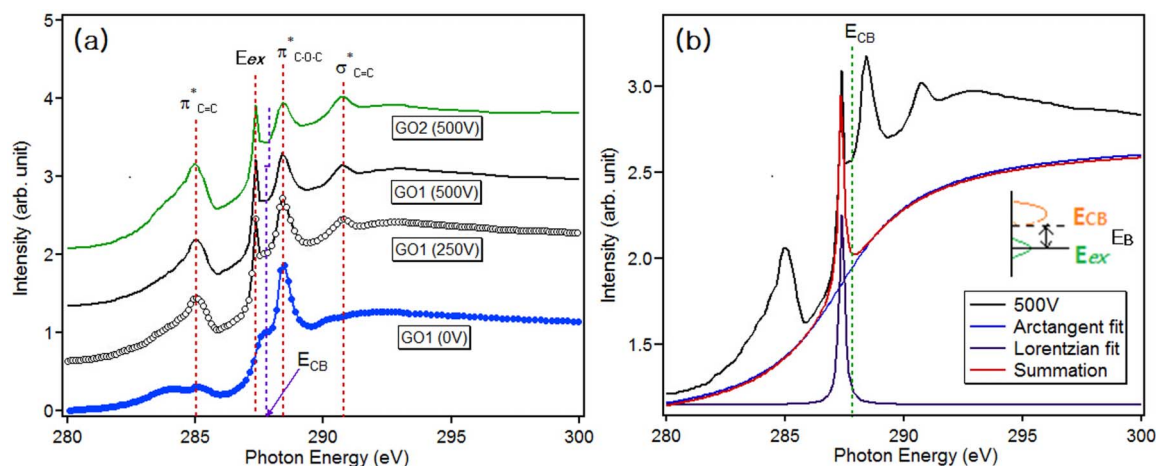
Figure 2 | XANES spectra of GOs. (a) High-resolution C K-edge XANES spectra of GO. (b) Fit of GO1 spectrum (500 V) with Lorentzian and Arctangent functions.

Table 1	O:C ratio of GO samples. The binding energy, the effective mass, and the Bohr radius of core excitons in GO sample are presented				
	O:C ratio	E_B	Bohr radius of exciton (a_x)	Effective mass (μ)
GO1	0.35	350 meV	6.23 Å	0.196 m_0
GO2	0.38	500 meV	4.36 Å	0.28 m_0

on the surface of GO, i.e. the proportion of the reacted regions increases while that of the unreacted regions in GO diminishes. Therefore, an increasing O:C ratio will yield more boundary walls, leading to stronger quantum confinement effects.

Valence excitons have been more widely studied than core excitons, and are different from core excitons in the following ways. First, the binding energy of a valence exciton is smaller than that of a core exciton. Second, electron-hole interactions are generally neglected when discussing valence band optical properties in a valence exciton. Although the valence exciton is generally investigated by luminescence methods, it is difficult to validate the presence of such an exciton in GO owing to strong charging. Instead, to corroborate the formation of a valence exciton in the unreacted regions of GO, first-principles calculations were carried out using a many-body perturbation theory approach based on a three-step procedure[17]. For the calculation, we constructed a GO structure with epoxy groups as the confinement wall, containing an unreacted GO area of 1.5 nm × 2.6 nm (Figure 3a). We assumed that the unreacted regions in Figure 1c are similar to diamond-shaped GNRs separated by epoxy group walls.

Figure 3a illustrates this simulated structure of GO, where the unit cell size is defined by the confinement wall boundaries. Although hydrogen and oxygen atoms comprise the confinement walls in these carbon domains, and hydrogen acts as a hard wall (see the Supplementary Information, Figure S2) while oxygen offers a much softer boundary, this calculation assumed that the walls were formed exclusively from oxygen. This assumption is tenable because the experimental GO samples have a low coverage of chemical groups within graphitic regions. In addition, the graphitic domain size is as large as 2.0 nm. GO samples can be clearly discriminated based on the ribbon morphology. Thus, one can assume that the difference between the hydrogen and oxygen in the calculation is negligibly small.

The ground state electronic properties of the structure were calculated within the local density approximation (LDA) using the Abinit code with separable norm-conserving pseudopotentials and a plane-wave basis set[18]. A kinetic energy cut-off of 50 Ry and 121 k-points were employed. Each atomic structure was fully relaxed until forces acting on atoms were less than 0.01 eV/Å. Next, the quasi-particle corrections to the LDA eigenvalues were computed using a screened Coulomb potential and the Green's function for the self-energy operator according to the GW approximation. In this procedure, LDA wave functions acted as good approximations to those for quasiparticles, while screening was treated within the plasmon-hole approximation[19] by solving the Bethe-Salpeter (BS) equation,

$$(E_{ck} - E_{vk})A^S_{vck} + \sum_{k'v'c'} <vck|K^{eh}|v'c'k'> A^S_{v'c'k'} = \Omega^S A^S_{vck},$$

where A^S_{vck} is the exciton wave function, K^{eh} is the electron-hole coupling kernel, Ω^S is the excitation energy, and E_{ck} and E_{vk} are the quasiparticle energies of the electron and hole states, respectively. Since a supercell method was employed in these calculations, a rectangular-shaped truncated Coulomb interaction was applied in order to eliminate the image effect between adjacent supercells. In this way, the result mimics isolated GNRs[20,21]. The valence and conduction bands each featured 10 band levels near the Fermi level in our calculation. All of the GW-BS calculations were performed using the Yambo code[22].

The inset of Figure 3a illustrates the simulated electronic absorption spectrum, where the first transition peak appears at 0.07 eV. The valence band maximum (VBM) and conduction band minimum (CBM) are shown in Figure 3b, where a confined sp^2 carbon domain is dominant in both the VBM and CBM. The valence exciton wave functions are confined along the edges of the unit cell in the VBM, while the wave functions are confined to the corners of the unit cell in the CBM. The GW-corrected band gap is about 0.61 eV. The calculated valence exciton binding energy, E_{VB}, is ca. 0.54 eV.

The size of the GO structure in this simulation is much smaller than that of the real GO structures shown in the TEM images. However, for an exciton formed within a carbon domain whose width is less than 2 nm, a scaling power law can be used to calibrate exciton parameters, including E_B, according to the size of a given graphitic structure[23]. For example, GNRs can be categorized into three families, 3p, 3p + 1 and 3p + 2[23], where p is a positive integer and indicates the number of dimer lines across the ribbon width. A power law is associated with each family, with exponents −0.60, −0.73, and −0.55, respectively. A power law with these corresponding exponents is used to calculate E_{VB}.

When the width of a GNR is larger than 2 nm, E_{VB} changes slightly and begins to converge toward the limits, 0.75 eV for the 3p and 3p + 1 families, and 0.45 eV for the 3p + 2 family (see Supplementary Information, Figure S2). For the GO structure simulation, shown in Figure 3a, the average domain width is (1.5 nm + 2.6 nm)/2 ≈ 2.0 nm, which is close to the critical size limit with a converged E_B (see Supplementary Information). E_{VB} of the simulated GO structure is equal to 0.54 eV across an average width of 2.0 nm,
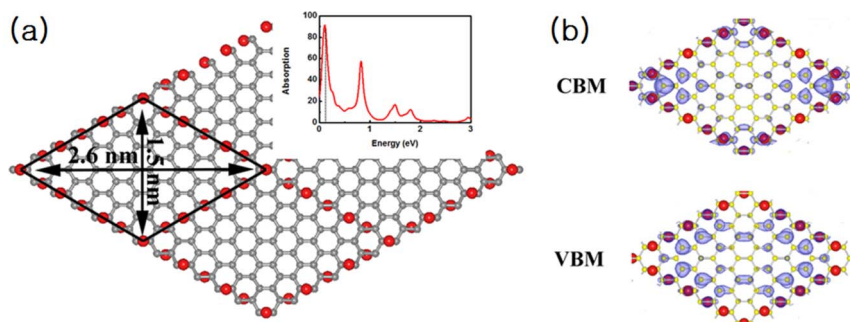
Figure 3 | Valence exciton wavefunctions in the graphitic region of GO. (a) Atomic structure for GO. The unit cell is marked by the black-line boundary which has a size of about 1.5 nm × 2.6 nm. The gray and red colors represent the carbon and oxygen atoms, respectively. The inset is the simulated electronic absorption spectrum. (b) The conduction band minimum (CBM) and valence band maximum (VBM) for the GO structure given in Figure 3a. The exciton wave functions are represented as purple.
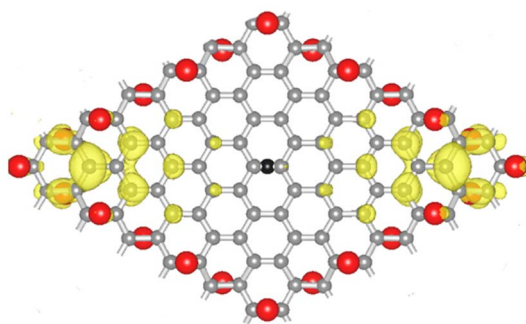
Figure 4 | Valence exciton wavefunction for the first transition peak shown in the inset of Figure 3(a). The gray and red colors represent the carbon and oxygen atoms, respectively. The yellow exciton wavefunctions are localized at the two corners along the x-axis, while the small wavefunction in the CBM of Figure 3b along the y-axis disappeared. A hole (black spot) is fixed in the middle of π bond. The iso-value is 0.02.

close to that of the 3p + 2 family for the GNRs ($E_{VB} \sim 0.45$ eV). For the GO structure, for which the domain size is larger than 2.0 nm, the converged E_{VB} is estimated to be close to the E_{VB} limit of 3p + 2 GNRs, or 0.45 eV (see Supplementary Information). The computational results verify that the valence exciton is indeed generated in the graphitic domain of GO and that the binding energy of the valence exciton is inversely proportional to the width of GNRs.

The simulated valence exciton wave function for the first transition peak is shown in Figure 4. This wavefunction is localized in the sp² carbon domains. Such a feature is common to valence excitons generated in other graphene-based structures displaying quantum confinement, such as GNRs[23–26]. The valence exciton in GNRs is caused by the edge confinement effect in graphene. Since the valence exciton in GO is formed in graphitic regions like anthracene[27,28], it has clear non-Frenkel characteristics. In addition to the ribbon structure, the simulation performed here can also be applied to GO with nano-graphitic regions. The structure of Figure 3(a) is quadrilateral, similar to that found for nano-graphitic islands. Thus, wherever GO samples contain nanoscale sp²-domains, the binding strength of valence excitons will exhibit similar characteristics.

Discussion

Returning to the optoelectronic properties of GO, it is well known that GO exhibits steady-state photoluminescence (PL) and that this PL appears in graphitic regions in GO[29,30]. The PL in GO is dominated by optical emission at 600 nm. With the increased chemical reduction of GO, the peak emission wavelength shifts from 600 nm to 400 nm[29]. The PL process in GO has been explored using time-resolved PL (TRPL) experiments and the associated data were decomposed into three exponential decay processes[29]. However, the nature of this PL process has not yet been fully understood. Since the origin of the PL is likely to be related to the valence exciton and PL experiments are generally used to measure the lifetime of valence excitons in semiconductors, TRPL experiments were performed to investigate the luminescent properties of GO.

GO samples were excited at $\lambda_{ex} = 400$ nm. Emission data using $\lambda_{em} = 600$ nm were collected with time. Figure 5 (a) illustrates the TRPL of GOs with time. GO1 shows a slower relaxation than GO2. The PL spectra of both GO samples shows a multi-exponential decay, which was decomposed into three exponential components: 187, 1415, and 6090 ps for GO1, and 33, 467, and 5870 ps for GO2. These PL results also show similar behavior with other GO materials previously reported. As the graphitic region becomes smaller with a higher oxidation, the emission decays faster, which is also common in quantum dot materials[31]. Figure 5 (b) and (c) are the schematic models for GO1 and GO2, respectively. The origin of PL is presumably related to the presence of the valence exciton supported by the calculation results.

We have investigated the structural properties of GO with TEM, revealing that two types of regions co-exist in GO. To study quantum confinement in GO, high-resolution XANES was performed. XANES spectra show that core excitonic states are formed in GO. As the O:C ratio of GO increases, the binding energy of the core exciton increases. First-principles calculations show that electrons in GO are confined in unreacted regions and the binding energy of valence excitons is inversely proportional to the size of unreacted regions. Electrons in unreacted regions of GO are confined and, as a result, core/valence excitonic states are induced. Furthermore, the binding energy of the core exciton and the relaxation time of the valence exciton in GO can be tuned by controlling the degree of oxidation in GO. These findings suggest that GO has potential applications in two dimensional optoelectronic devices.

Methods

Sample preparation. GO samples were prepared by the Brodie process. Graphite (5 g, 99.995% purity, 45 μm, Aldrich) was added to fuming nitric acid (65.5 mL). After cooling the mixture in an ice bath, $KClO_3$ (25.0 g) was slowly added while stirring for 30 minutes. The mixture was kept at this temperature for 3 days. It was then transferred into cold deionized water (1 L), the solution was immediately
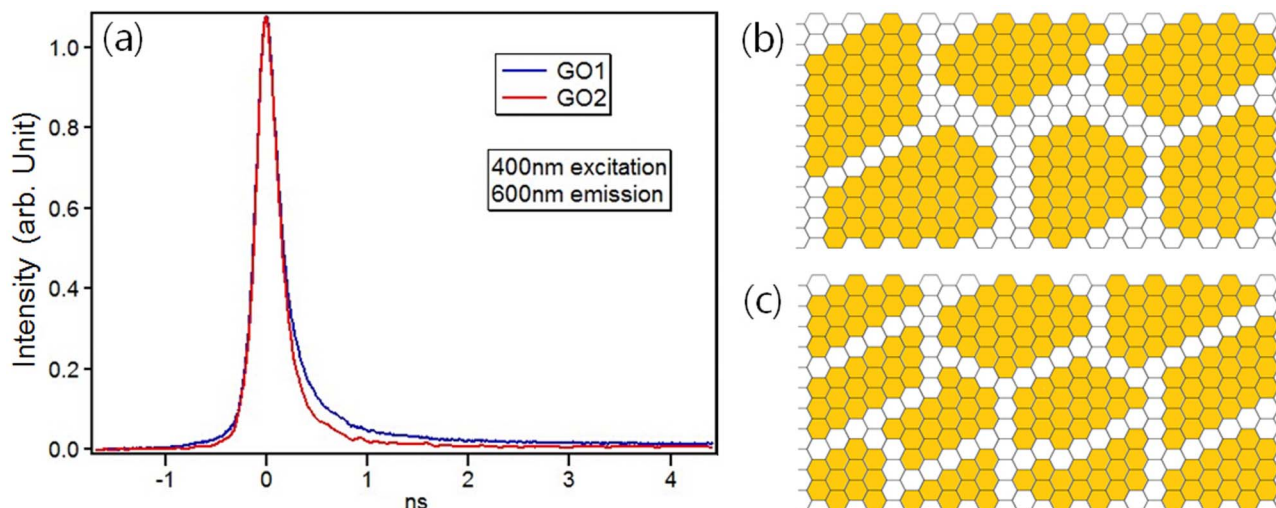
Figure 5 | Time-resolved PL spectra of GOs. (a) TRPL spectra of GO samples. (b)–(c) schematic GO models for GO1 and GO2, respectively. The yellow regions represent graphitic regions.

centrifuged and the residual powder washed. The residual powder was dried overnight at 70°C and the procedure was repeated.

Morphology characterization. To characterize the morphological properties of GO, we used a FEI Philips Tecnai 20 transmission electron microscope (TEM). The elemental composition of the samples was identified by energy dispersive X-ray (EDX) analysis.

XANES experiments. The samples were also characterized by high-resolution X-ray absorption near edge structure (XANES) spectroscopy, which was performed on the 2A undulator beamline at PAL in Korea. The XANES spectra were acquired at room temperature using a total electron yield (TEY) detection mode in order to minimize charging effects.

Time-resolved photoluminescence. The dynamics of luminescent properties of GO was investigated by time resolved photoluminescence. 400 nm excitation pulses were generated from an optical parametric amplifier, pumped by a 1 kHz, 150 fs regenerative amplifier. The PL signal was time-resolved using an Optronis Optoscope streak camera system with a temporal resolution of 6 ps.

1. Novoselov, K. S. et al. Electric Field Effect in Atomically Thin Carbon Films. *Science* **306**, 666–669 (2004).
2. Gundra, K. & Shukla, A. Theory of the electro-optical properties of graphene nanoribbons. *Phys. Rev. B* **83**, 075413 (2011).
3. Osella, S. et al. Graphene Nanoribbons as Low Band Gap Donor Materials for Organic Photovoltaics: Quantum Chemical Aided Design. *ACS Nano* **6**, 5539–5548 (2012).
4. Liu, L. et al. Graphene oxidation:Thickness-dependent etching and strong chemical doping. *Nano Lett.* **8**, 1965–1970 (2008).
5. He, H., Klinowski, J., Forster, M. & Lerf, A. A new structural model for graphite oxide. *Chem. Phys. Lett.* **287**, 53–56 (1998).
6. Lerf, A., He, H. Y., Forster, M. & Klinowski, J. Structure of Graphite Oxide Revisited. *J. Phys. Chem. B* **102**, 4477–4482 (1998).
7. Lee, D. W. et al. The Structure of Graphite Oxide: Investigation of Its Surface Chemical Groups. *J. Phys. Chem. B* **114**, 5723–5728 (2010).
8. Brodie, B. C. On the Atomic Weight of Graphite. *Philos. Trans. R. Soc.* **149**, 249–259 (1859).
9. Bao, W. et al. Controlled ripple texturing of suspended graphene and ultrathin graphite membranes. *Nat. Nanotechnol.* **4**, 562–566 (2009).
10. Loh, K. P., Bao, Q., Ang, P. K. & Yang, J. The chemistry of graphene. *J. Mater. Chem.* **20**, 2277–2289 (2010).
11. Coffman, F. L. et al. Near-edge x-ray absorption of carbon materials for determining bond hybridization in mixed $sp^2 = sp^3$ bonded materials. *Appl. Phys. Lett.* **69**, 568–570 (1996).
12. Francis, J. T. & Hitchcock, A. P. Inner-shell spectroscopy of p-benzoquinone, hydroquinone, and phenol: distinguishing quinoid and benzenoid structures. *J. Phys. Chem.* **96**, 6598–6610 (1992).
13. Skytt, P. et al. Angle-resolved soft-x-ray fluorescence and absorption study of graphite. *Phys. Rev. B* **50**, 10457–10461 (1994).
14. Stohr, J. NEXAFS Spectroscopy. Springer-Verlag, Berlin, (1992).
15. Knupfer, M. Exciton binding energies in organic semiconductors. *Appl. Phys. A* **77**, 623–626 (2003).
16. Jeong, H., Jin, M. H., An, K. H. & Lee, Y. H. Structural Stability and Variable Dielectric Constant in Poly Sodium 4-Styrensulfonate Intercalated Graphite Oxide. *J. Phys. Chem. C* **113**, 13060–13064 (2009).
17. Onida, G., Reining, L. & Rubio, A. Electronic excitations: density-functional versus manybody Green's-function approaches. *Rev. Mod. Phys.* **74**, 601–659 (2002).
18. Gonze, X. ABINIT: First-principles approach to material and nanosystem properties. *Computer Physics Communications* **180**, 2582–2615 (2009).
19. Godby, R. W. & Needs, R. J. Metal-insulator transition in Kohn-Sham theory and quasiparticle theory. *Phys. Rev. Lett.* **62**, 1169–1172 (1989).
20. Ismail-Beigi, S. Truncation of periodic image interactions for confined systems. *Phys. Rev. B* **73**, 233103 (2006).
21. Rozzi, C. A. et al. Exact Coulomb cutoff technique for supercell calculations. *Phys. Rev. B* **73**, 205119 (2006).
22. Marini, A., Hogan, C., Gruning, M. & Varsano, D. Yambo: An ab initio tool for excited state calculations. *Computer Physics Communications* **180**, 1392–1403 (2009).
23. Zhu, X. & Su, H. B. Scaling of Excitons in Graphene Nanoribbons with Armchair Shaped Edges. *J. Phys. Chem. A* **115**, 11998–12003 (2011).
24. Zhu, X. & Su, H. B. Excitons of Edge and Surface Functionalized Graphene Nanoribbons. *J. Phys. Chem. C* **114**, 17257–17262 (2010).
25. Prezzi, D. et al. Optical properties of graphene nanoribbons: The role of many-body effects. *Phys. Rev. B* **77**, 041404 (2008).
26. Yang, L., Cohen, M. L. & Louie, S. G. Excitonic Effects in the Optical Spectra of Graphene Nanoribbons. *Nano Lett.* **7**, 3112–3115 (2007).
27. Kenkre, V. M. & Schmid, D. Coherence in singlet-exciton motion in anthracene crystals. *Phys. Rev. B* **31**, 2430–2436 (1985).
28. Smith, G. C. Triplet Exciton Phosphorescence in Crystalline Anthracene. *Phys. Rev.* **166**, 839–847 (1968).
29. Eda, G. et al. Blue Photoluminescence from Chemically Derived Graphene Oxide. *Adv. Mater.* **22**, 505–509 (2010).
30. Lu, J. et al. One-Pot Synthesis of FluorescentCarbon Nanoribbons, Nanoparticles, and Graphene by the Exfoliation of Graphite in Ionic Liquids. *ACS Nano* **3**, 2367–2375 (2009).
31. Hong, S. et al. Time resolved photoluminescence of size-controlled ZnO nanorods. *Appl. Phys. Lett.* **83**, 4157–4159 (2003).

Acknowledgements

Author contributions

D.L. managed the project, prepared the samples, carried out TRPL experiments, analyzed the data and wrote the manuscript; J.S. and H.L. performed XANES experiments; X.Z. and H.S. carried out the theoretical calculations and analysis of exciton; T.S. carried out P.L. experiments; J.L., H.J.S., J.M.C. and J.L. contributed to discussion, data analyses or sample preparation throughout the project.

Additional information